recycling

MDPI

Article

Synergetic Treatment of BOF Slag and Copper Slag via Oxidation–Magnetic Separation for $MgFe_2O_4$ Preparation and Non-Magnetic Slag Stabilization

Bowen Cao [1,2], Nan Wang [2,*] and Min Chen [1,2]

[1] Key Laboratory for Ecological Metallurgy of Multimetallic Ores (Ministry of Education), Northeastern University, Wenhua Road, Heping District, Shenyang 110819, China; 18586128464@163.com (B.C.); chenm@smm.neu.edu.cn (M.C.)
[2] School of Metallurgy, Northeastern University, Wenhua Road, Heping District, Shenyang 110819, China
* Correspondence: wangnan@mail.neu.edu.cn; Tel.: +86-24-8368-7052

Abstract: This study proposes a synergistic treatment method for BOF slag and copper slag via oxidation–magnetic separation, with the dual goals of preparing $MgFe_2O_4$ magnetic material and stabilizing the non-magnetic slag. The effects of copper slag addition, the oxidation temperature and the oxidation time on the phase transformation and $MgFe_2O_4$ morphology during the oxidation process are investigated. The results show that copper slag addition can release the simple iron oxides of FeO and Fe_2O_3 from iron-containing phases from BOF slag and copper slag, promoting the synthesis of $MgFe_2O_4$. Furthermore, the oxidation temperature and oxidation time have a significant influence on the size of the $MgFe_2O_4$ particles. To obtain the $MgFe_2O_4$ magnetic material, the optimum oxidation parameters were used, with an oxidation degree of Fe^{2+} of 95.85% and a yield of $MgFe_2O_4$ of 90.31%. In addition, the main phase of non-magnetic slag was Ca_2SiO_4, and both free CaO and free MgO from BOF slag were eliminated, indicating a potential application in construction materials. This technology maximizes resource utilization and the valorization of metallurgical solid waste.

Keywords: BOF slag; copper slag; oxidation–magnetic separation; $MgFe_2O_4$ preparation; non-magnetic slag stabilization

check for updates

Academic Editor: Jack Groppo

Received: 27 February 2025
Revised: 12 April 2025
Accepted: 24 April 2025
Published: 1 May 2025

Citation: Cao, B.; Wang, N.; Chen, M. Synergetic Treatment of BOF Slag and Copper Slag via Oxidation–Magnetic Separation for $MgFe_2O_4$ Preparation and Non-Magnetic Slag Stabilization. *Recycling* **2025**, *10*, 81. https://doi.org/10.3390/recycling10030081

Copyright: © 2025 by the authors. Licensee MDPI, Basel, Switzerland. This article is an open access article distributed under the terms and conditions of the Creative Commons Attribution (CC BY) license (https://creativecommons.org/licenses/by/4.0/).

1. Introduction

BOF slag—a major type of solid waste in the steel industry, with a yearly output of roughly 120 million tons in China—is currently landfilled without proper treatment, causing environmental problems [1–4]. The utilization rate of BOF slag is approximately 30%, and it is mostly used in the production of cement concrete and road paving. However, the high hardness of BOF slag makes it difficult to crush due to the presence of iron-containing phases, which raises the processing cost [5,6]. Furthermore, the phases of free CaO and free MgO in BOF slag cause volume expansion, restricting its application in construction materials [7–9]. In recent years, the comprehensive treatment of BOF slag has aimed to recover the iron resource and utilize the non-magnetic slag, and pyrometallurgy is the preferred method due to its lower level of secondary pollution than hydrometallurgy [10,11]. At present, iron is extracted from BOF slag mostly by the reduction process, and many studies show that high-efficiency iron recovery from BOF slag is dependent on the appropriate SiO_2-containing composition adjustment of BOF slag. For example, Guo et al. [12] used kaolin and carbon powder as an additive mixture to adjust the BOF slag's basicity,

and the results showed that 95% of the iron had been recovered and the non-magnetic slag could be used as supplementary cementitious material. Hao et al. [13] proposed to optimize the modification of converter slag and blast furnace slag using dust removal ash as a reducing agent; as a result, the goal of recovering iron resources from the converter slag was achieved. Dai et al. [14] developed a technical route for BOF slag's large-scale utilization, using fly ash as a modifier and coal powder as a reducing agent to recover iron resources. Although the iron recovery rate of BOF slag is significant when a carbonaceous reductant is used, the reduction method suffers from certain limitations. Not only does the process inevitably emit greenhouse gases, i.e., CO_2, but the phosphorus in BOF slag is also reduced and dissolves in the metallic iron, limiting the application of this metallic iron.

On the other hand, the metallic iron of BOF slag can be recovered by magnetic separation, but iron oxides are non-magnetic, resulting in lower iron recovery. Therefore, some investigations have concentrated on iron recovery in BOF slag using oxidation methods. Lan et al. [15] realized the transformation from weak magnetic iron oxides to the strong magnetic magnesia–iron ($MgFe_2O_4$) spinel phase in BOF slag through oxidation experiments, and they optimized the process parameters. Xue et al. and He et al. [16,17] proposed an oxidation method for BOF slag treatment with SiO_2 as a modifier. The iron-containing phases in BOF slag could be transformed to $MgFe_2O_4$ through the oxidation process, and the magnetic separation efficiency was better than that of direct separation without any treatment. However, the aforementioned methods require the reheating of the cold BOF slag to a high temperature, from 1200 to 1400 °C in air, which not only wastes enormous quantities of heat carried by the hot BOF slag [18] but also extends the oxidation time and increases the treatment cost. As a result, it is necessary to develop a low-energy and ecologically acceptable treatment method for BOF slag.

Copper slag is a typical by-product of the copper smelting industry, containing approximately 30% SiO_2, and can be utilized as a SiO_2-containing modifier [19]. According to our earlier study [20], BOF slag and copper slag possess the capacity to act as modifiers for each other, facilitating the release of simple iron oxides from the complicated mineral phases in the two slags and enhancing the iron oxide activity. Furthermore, BOF slag contains both iron oxide and magnesium oxide, and the iron oxides in BOF slag are primarily found in dicalcium ferrite and RO phases. With the addition of copper slag to BOF slag, both the Fe_2O_3 in dicalcium ferrite in the BOF slag and the FeO in fayalite in the copper slag can be released, transforming the iron oxides in the two slags into a strong magnetic $MgFe_2O_4$ phase under oxygen and separating them by magnetic separation.

Spinel-type magnesium ferrite ($MgFe_2O_4$) has attracted a lot of attention in the fields of wastewater treatment, electrode composites and electromagnetic wave absorbers. Thus far, the solid-state reaction has been the main industrial production method for the preparation of $MgFe_2O_4$ [21–23]. However, the necessity of raw materials limits the large-scale preparation of $MgFe_2O_4$ and the process carries high costs and causes environmental pollution. Therefore, it is preferable to prepare $MgFe_2O_4$ directly via the synergistic treatment of metallurgical waste.

The waste heat of hot BOF slag tapped from the converter is the largest secondary energy source that may be reused, while the synergetic oxidation process of BOF slag and copper slag is exothermic. As a result, utilizing waste heat from hot BOF slag and oxidation reaction heat will greatly reduce the energy consumption during the synergetic oxidation process.

In this work, a synergetic treatment method for BOF slag and copper slag is proposed, using oxidation–magnetic separation to prepare $MgFe_2O_4$ magnetic material while also stabilizing the non-magnetic slag. The effects of copper slag addition, the oxidation temperature and the oxidation time on the phase transformation and $MgFe_2O_4$ morphology were

investigated, and the oxidation degree of Fe^{2+} and the yield of $MgFe_2O_4$ were evaluated. The purpose of this innovative synergistic treatment of BOF slag and copper slag is to use industrial solid waste to prepare high-value commodities.

2. Results and Discussion

2.1. Phase Transformation and $MgFe_2O_4$ Morphology During Oxidation Process

2.1.1. Effect of Copper Slag Addition

Figure 1a,b show the XRD results and Rietveld refinement analysis of the oxidation slags with different copper slag additions at an oxidation temperature of 1450 °C and an oxidation time of 10 min. As shown in Figure 1a, the diffraction peaks of the oxidation slags (phase 1) and $MgFe_2O_4$ in PDF#96-900-1451 correspond well in terms of the diffraction angle and height, suggesting that $MgFe_2O_4$ is formed. It can be observed that $Ca_2Fe_2O_5$ is exclusively present in the S0 sample, where no copper slag is added. Furthermore, the RO phase in the BOF slag disappears after the oxidation process, indicating that the FeO in the RO phase can be oxidized to Fe_2O_3 and forms $MgFe_2O_4$ in situ under an oxidizing atmosphere, as shown in Equation (1). The addition of copper slag resulted in a significant enhancement in the diffraction peak intensity of $MgFe_2O_4$ in the S1–S3 samples in comparison to the S0 sample. Furthermore, the diffraction peak intensity of $Ca_2Fe_2O_5$ in BOF slag and Fe_2SiO_4 in copper slag underwent complete disappearance. The synergistic modification between the two slags via the reactions shown in Equation (2) was found to promote the release of simple iron oxides from the complex iron-containing mineral phases in the two slags, thereby enhancing the activity of the iron oxides and facilitating the formation of $MgFe_2O_4$, as shown in Equation (3). In addition, the XRD patterns of the S1–S3 samples show no diffraction peaks for free CaO and free MgO in BOF slag. The results indicate that the synergistic oxidation of BOF slag and copper slag is favorable for $MgFe_2O_4$ formation and BOF slag stabilization [24,25].

$$4FeO + O_2 + 2MgO = 2MgFe_2O_4 \quad (1)$$

$$Ca_2Fe_2O_5 + Fe_2SiO_4 = Ca_2SiO_4 + 2FeO + Fe_2O_3 \quad (2)$$

$$Fe_2O_3 + MgO = MgFe_2O_4 \quad (3)$$

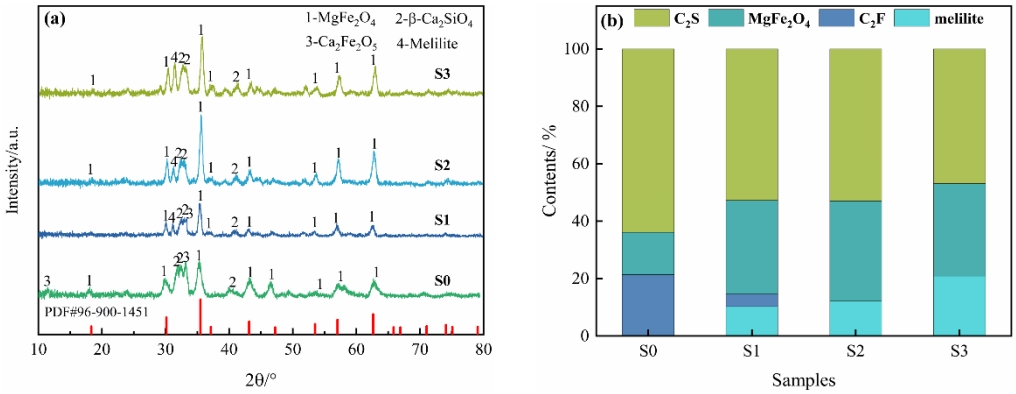


Figure 1. XRD patterns of the oxidation slags with different copper slag additions: (**a**) XRD analysis; (**b**) Rietveld refinement analysis.

Figure 1b shows the results of the Rietveld refinement analysis of the XRD patterns [26,27], which demonstrates that the greatest $MgFe_2O_4$ content of 32.82% is achieved with the addition of 10% copper slag. However, when 15% copper slag is added, the content of melilite ($Ca_2MgSi_2O_7$ and $Ca_2Al_2SiO_7$) gradually increases, while the content of $MgFe_2O_4$

decreases, which is not conducive to $MgFe_2O_4$ formation. Figure 2 and Table 1 show the SEM-EDS analysis of the oxidation slags. As shown in Figure 2(a1,a2), the iron-containing phases in the S0 sample are $MgFe_2O_4$ and $Ca_2Fe_2O_5$, and a large number of small-faced $MgFe_2O_4$ crystals form clusters of crystals. Furthermore, Figure 2(b1,b2) show that the $MgFe_2O_4$ in the S1 sample can be mainly divided into two different morphologies, namely honeycomb and clusters [28], and Ca_2SiO_4 and $Ca_2Fe_2O_5$ are closely dispersed around $MgFe_2O_4$, preventing magnetic phase separation. As shown in Figure 2(c1,c2,d1,d2), with an increase in copper slag addition, the $Ca_2Fe_2O_5$ phase disappears, and many small $MgFe_2O_4$ crystals gradually grow and aggregate into large polygonal crystals, with particles sizes of nearly 60 μm, indicating that the addition of copper slag obviously promotes the agglomeration and growth of $MgFe_2O_4$ [29]. However, the amount of melilite increases with the addition of 15% copper slag, as shown in Table 1. Melilite not only contains little Fe, but it also results in a decrease in Mg involved in the reaction, which is not conducive to the formation of $MgFe_2O_4$.

Moreover, all β-Ca_2SiO_4 phases of the oxidation slags contain phosphorus elements, suggesting that phosphorus elements do not migrate during the process. According to the literature [30,31], C2S exists in the crystal form of β-Ca_2SiO_4 rather than γ-Ca_2SiO_4, because phosphorus stabilizes β-Ca_2SiO_4 by replacing $[SiO4]^{4-}$ groups with $[PO4]^{3-}$ groups to form a Ca_2SiO_4–$Ca_3(PO_4)_2$ solid solution. This prevents the volume instabilities caused by the transformation to γ-Ca_2SiO_4 and the phosphorus enrichment of $MgFe_2O_4$.

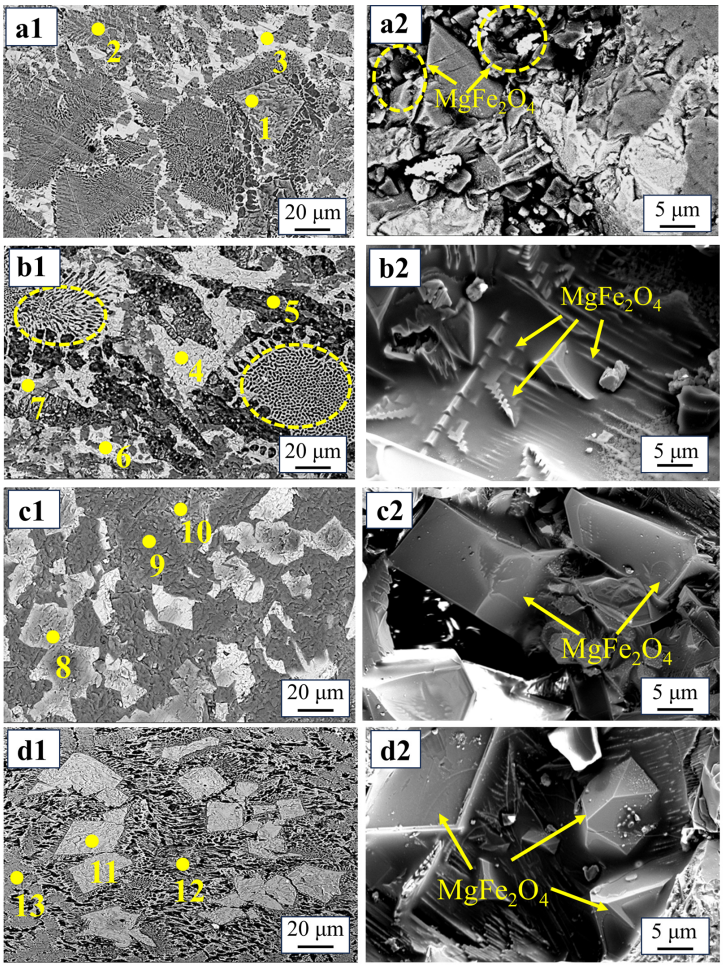


Figure 2. Morphologies of $MgFe_2O_4$ with different copper slag additions: (**a1**,**a2**)—S0, 0%; (**b1**,**b2**)—S1, 5%; (**c1**,**c2**)—S2, 10%; (**d1**,**d2**)—S3, 15%.

Table 1. Atomic percentages of the spectrum points corresponding to Figure 2 (wt %).

Sample	Point	Phase	O	Mg	Fe	Ca	Si	Mn	Al	P
	1	$MgFe_2O_4$	52.04	15.64	29.13	/	/	2.14	1.05	/
S0	2	Ca_2SiO_4	43.66	/	0.84	37.20	16.70	/	0.36	1.23
	3	$Ca_2Fe_2O_5$	50.80	/	21.48	23.34	3.22	/	1.16	/
S1	4	$MgFe_2O_4$	57.33	13.59	26.12	/	/	1.40	1.56	/
	5	Ca_2SiO_4	57.37	/	/	25.35	13.62	/	/	1.66
	6	$Ca_2Fe_2O_5$	44.94	/	23.69	28.63	1.52	/	1.22	/
	7	Melilite	52.21	7.55	5.03	16.28	10.39	/	8.54	/
S2	8	$MgFe_2O_4$	49.57	15.57	31.45	/	/	1.68	1.73	/
	9	Ca_2SiO_4	58.30	/	0.77	27.50	12.43	/	/	0.99
	10	Melilite	48.15	8.28	6.90	15.28	10.50	0.61	10.28	/
S3	11	$MgFe_2O_4$	46.74	13.92	31.50	/	/	1.74	6.10	/
	12	Ca_2SiO_4	54.20	/	0.64	30.21	13.20	/	/	1.75
	13	Melilite	43.84	7.51	10.48	18.77	9.23	/	10.17	/

Figure 3 shows that, as the addition of copper slag rose from 0% to 5%, the oxidation degree of Fe^{2+} and the yield of $MgFe_2O_4$ increased dramatically. The formation of $MgFe_2O_4$ increased significantly from 60.32% to 86.57%, whereas the oxidation degree of Fe^{2+} remained roughly constant at 95.85% when the copper slag addition was greater than 10%. As a result, 10% copper slag addition was chosen for the subsequent experiments.

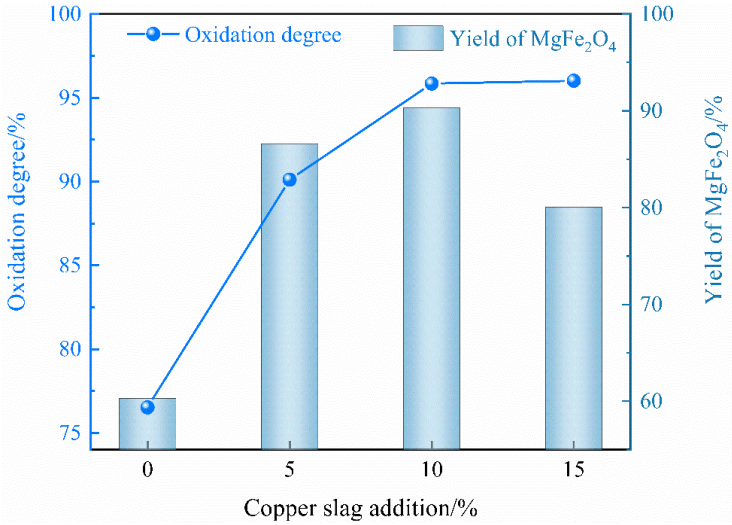


Figure 3. Effects of copper slag addition on the oxidation degree of Fe^{2+} and the yield of magnetic $MgFe_2O_4$.

2.1.2. Effect of Oxidation Temperature

Figure 4 depicts the XRD results of the oxidation slags at different temperatures under the parameters of 10% copper slag addition and a 10 min oxidation period. The phases in the oxidation slags are β-Ca_2SiO_4, $MgFe_2O_4$ and melilite. The diffraction peak of $MgFe_2O_4$ increases initially and then decreases as the temperature increases, whereas the diffraction peak of melilite increases dramatically, presumably due to the Fe and Mg elements decomposing from $MgFe_2O_4$, forming melilite at high temperatures.

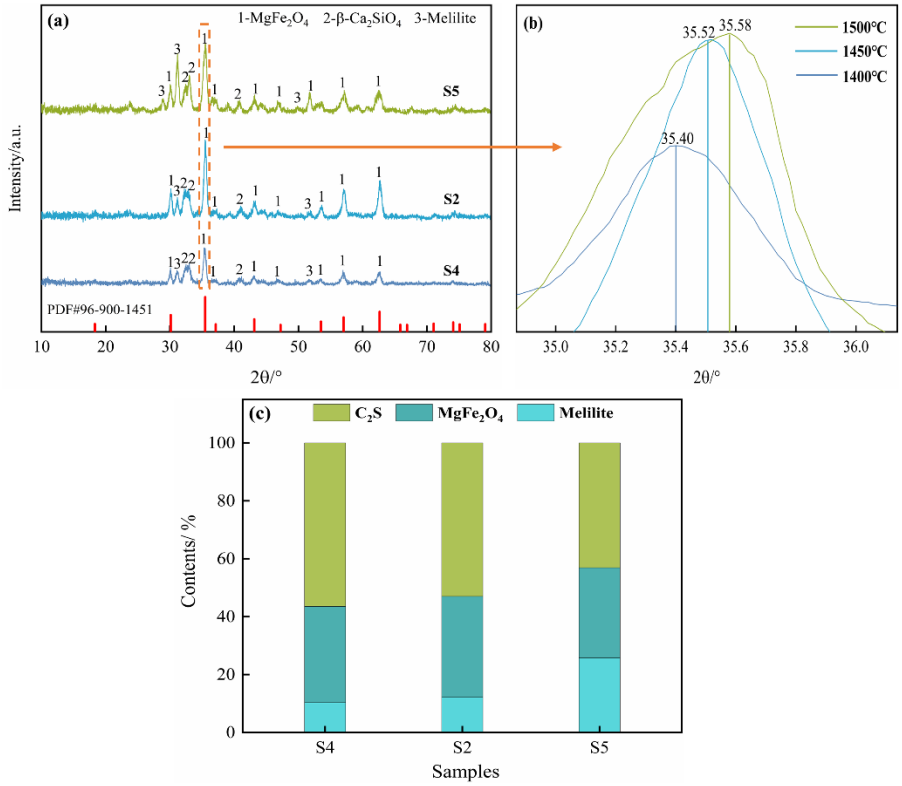


Figure 4. XRD patterns of the oxidation slags at different temperatures: (**a**) XRD analysis; (**b**) 34.8° to 36.2° magnified image; (**c**) Rietveld refinement analysis.

Furthermore, together with the Rietveld refinement analysis, as shown in Figure 4c, it is found that the greatest content of $MgFe_2O_4$ is 34.91% at 1450 °C. Figure 4b depicts an enlarged version of the dotted line area in Figure 4a. According to Bragg's law [32], the relationship between the diffraction angle and interplanar spacing is as shown in Equation (6):

$$2d \sin \theta = n\lambda \quad (4)$$

where d is the interplanar spacing, θ is the diffraction angle, n is the diffraction order and λ is the wavelength of Cu-Kα radiation.

The diffraction angle shifts to greater angles as the interplanar separation decreases. The ionic radii of Fe^{3+} (0.64 Å) and Al^{3+} (0.51 Å) are similar, allowing Fe^{3+} to be replaced with Al^{3+}, causing the diffraction angle of $MgFe_2O_4$ to become higher. As the temperature increased, more Al^{3+} was dissolved in $MgFe_2O_4$, resulting in the diffraction angle of $MgFe_2O_4$ shifting to greater angles. The doping of Al^{3+} will affect the distribution of cations in $MgFe_2O_4$, which will change the magnetism. Meanwhile, higher melilite content will decrease the formation of magnetic $MgFe_2O_4$.

The microstructures of the oxidation slags at temperatures ranging from 1400 to 1500 °C are shown in Figure 5, while Table 2 shows the atomic percentages of the relevant spectral spots. The yield of $MgFe_2O_4$ obtained through magnetic separation is closely related to its particle size. As shown in Figure 5a, the magnetic phases develop into tiny dendritic crystals along the direction of the nucleus. The size of the $MgFe_2O_4$ particles increases with the temperature, reaching a maximum of 60 μm, suggesting that a higher temperature can promote the formation and growth of $MgFe_2O_4$. Table 2 shows that the $MgFe_2O_4$ phase contains more Al at 1500 °C, indicating that higher temperatures can replace Fe^{3+} with Al^{3+}. Therefore, an overly high oxidation temperature will inhibit the synthesis of $MgFe_2O_4$.

Table 2. Atomic percentages of the spectrum points corresponding to Figure 5 (wt %).

Sample	Point	Phase	O	Mg	Fe	Ca	Si	Mn	Al	P
S4	1	$MgFe_2O_4$	48.83	14.80	32.72	0.19	/	1.80	1.66	/
	2	Ca_2SiO_4	52.63	/	/	29.56	16.21	/	/	1.60
	3	Melilite	47.28	8.97	6.37	18.73	9.44	/	9.21	/
S5	4	$MgFe_2O_4$	53.18	13.10	23.32	/	/	1.55	8.85	/
	5	Ca_2SiO_4	51.91	/	0.32	30.51	15.74	/	/	1.52
	6	Melilite	41.11	9.46	12.39	17.53	8.30	/	11.21	/

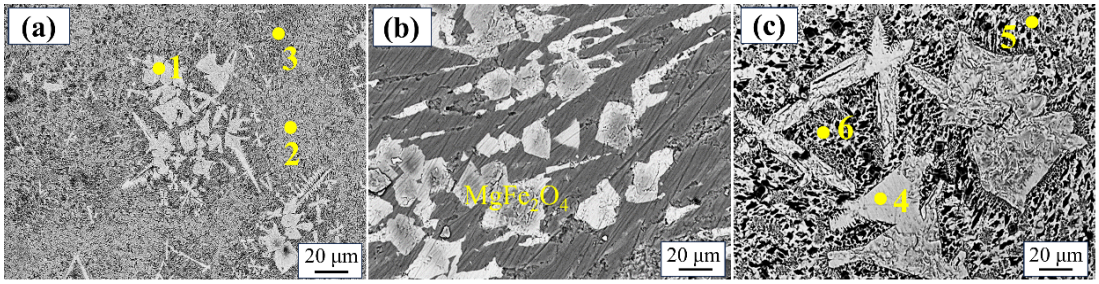


Figure 5. Morphologies of $MgFe_2O_4$ at different temperatures: (**a**)—S4, 1400 °C; (**b**)—S2, 1450 °C; (**c**)—S5, 1500 °C.

As shown in Figure 6, the influence of different oxidation temperatures on the oxidation degree of Fe^{2+} and the yield of $MgFe_2O_4$ is evident. It is observed that, with an increase in the oxidation temperature from 1400 to 1500 °C, there is a corresponding rise in the oxidation degree from 82.58% to 96.10%. This phenomenon can be attributed to the enhanced molecular diffusion rate at higher temperatures. An increase in the oxidation temperature can improve the kinetic conditions of the oxidation reaction and increase the mass transfer rate of iron ions (Fe^{2+} and Fe^{3+}) and O^{2-} in the slag, which is not only beneficial for the increase in the particle size of $MgFe_2O_4$, but also improves the yield of the magnetic phase in the magnetic separation process. Conversely, the yield of $MgFe_2O_4$ exhibits an initial increase, followed by a subsequent decrease, reaching a maximum value of 90.31% at an oxidation temperature of 1450 °C.

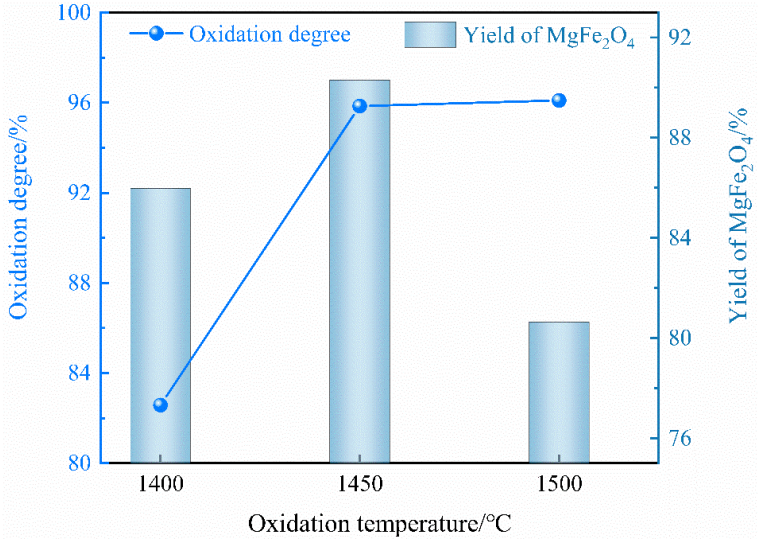


Figure 6. Effect of oxidation temperature on the oxidation degree of Fe^{2+} and the yield of magnetic $MgFe_2O_4$.

2.1.3. Effect of Oxidation Time

Figure 7a,b show the XRD results and Rietveld refinement analysis, respectively, after different oxidation times, with 10% copper slag addition and an oxidation temperature of 1450 °C. The diffraction peak intensity and the content of β-Ca_2SiO_4 and $MgFe_2O_4$ are basically consistent, but those of melilite gradually increase.

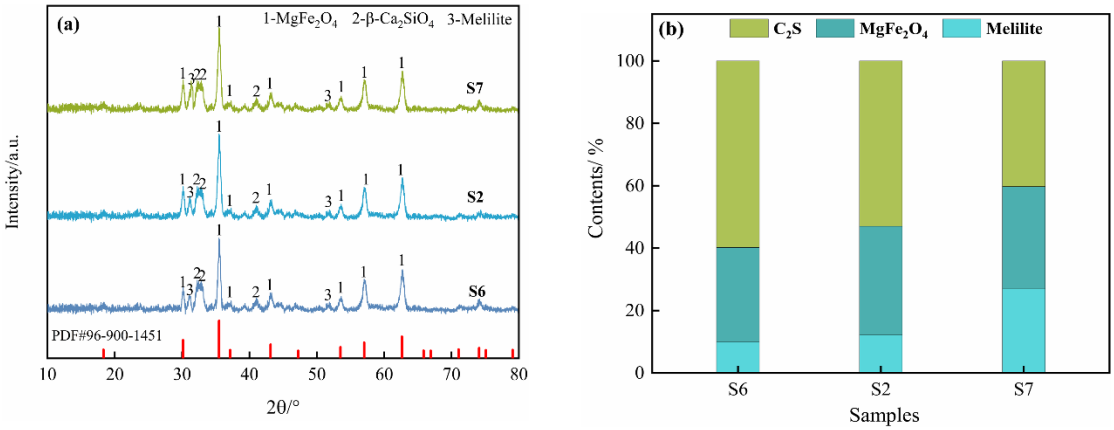


Figure 7. XRD patterns of oxidation slags at different times: (**a**) XRD analysis; (**b**) Rietveld refinement analysis.

Figure 8 and Table 3 show the microstructures and EDS results of the oxidation slags, respectively. Figure 8a–c demonstrate that the magnetic phases are $MgFe_2O_4$, with the amount and size of the particles obviously increasing with an increase in the oxidation time, indicating that the oxidation time is conducive to the growth of the $MgFe_2O_4$ phase. In addition, the presence of phases such as β-Ca_2SiO_4 and melilite has been confirmed through XRD analysis. Furthermore, it has been observed that, with an oxidation time of 5 min, the formation of dendritic crystallites of $MgFe_2O_4$ particles occurs, and these particles undergo further development into a regular octahedron with an increase in the oxidation time. Under the same amount of copper slag addition and oxidation temperature, an increase in the oxidation time improves the oxidation degree and also facilitates the aggregation and growth of $MgFe_2O_4$ particles. With the increase in the oxidation time, the microstructure of the $MgFe_2O_4$ particles transforms from fine crystalline to polyhedral, and the size of the particles increases significantly, which is beneficial for subsequent magnetic separation.

However, an increase in the melilite content has been observed to disrupt the phase growth of $MgFe_2O_4$ at an oxidation time of 15 min, resulting in a reduction in the magnetite size, thereby hindering the separation of the magnetic phases.

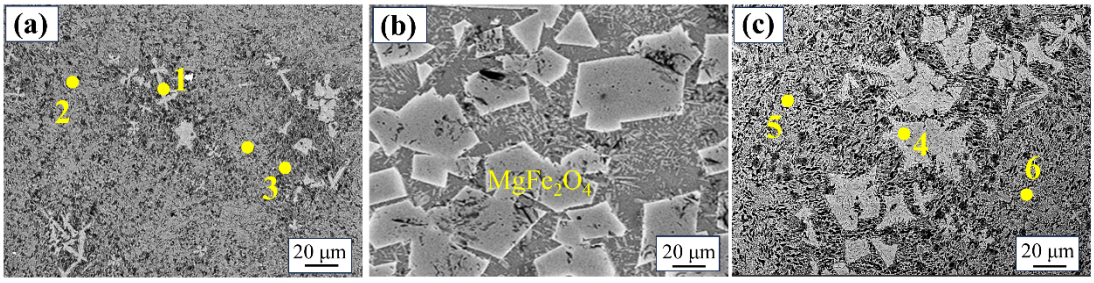


Figure 8. Morphologies of $MgFe_2O_4$ after different oxidation times: (**a**)—S6,5 min; (**b**)—S2, 10 min; (**c**)—S7, 15min.

Table 3. Atomic percentages of the spectrum points corresponding to Figure 8 (wt %).

Sample	Point	Phase	O	Mg	Fe	Ca	Si	Mn	Al	P
S6	1	$MgFe_2O_4$	54.46	13.52	28.63	/	/	1.69	1.70	/
	2	Ca_2SiO_4	51.93	/	0.22	30.66	15.46	/	/	1.73
	3	Melilite	42.98	6.41	6.17	20.39	15.58	/	8.47	/
S7	4	$MgFe_2O_4$	46.36	14.87	30.23	/	/	1.64	6.89	/
	5	Ca_2SiO_4	57.87	/	0.48	27.44	11.49	/	/	2.72
	6	Melilite	45.33	8.06	8.99	18.47	8.83	/	10.32	/

Figure 9 illustrates the impact of different oxidation times on the oxidation degree of Fe^{2+} and the yield of $MgFe_2O_4$. The oxidation degree increases significantly with increasing oxidation times from 5 to 10 min. Nevertheless, when the oxidation time is extended to 15 min, the oxidation degree demonstrates a gradual upward trend, suggesting that the majority of the Fe^{2+} in the oxidation slags has been oxidized to Fe^{3+}. Additionally, the yield of $MgFe_2O_4$ attained its maximum at 10 min, substantiating the recommendation of an oxidation time of 10 min.

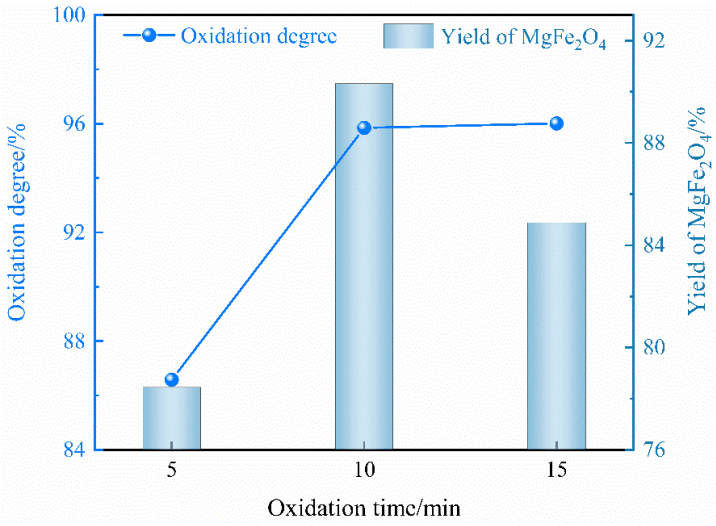


Figure 9. Effect of oxidation time on oxidation degree of Fe^{2+} and yield of magnetic $MgFe_2O_4$.

2.2. Magnetic Separation Product Analysis

Table 4 shows the chemical compositions of the oxidation slags. It can be seen that, with an increase in copper slag addition, there is almost no FeO in the oxidation slag, indicating that the oxidation reaction is completed, and the FeO in the BOF slag and copper slag is oxidized to Fe_2O_3. Figure 10 shows the XRD results of the magnetic product and non-magnetic slag of the S2 sample after magnetic separation. The main phase of the magnetic product is $MgFe_2O_4$. Furthermore, as shown in Table 5, the main chemical components of the magnetic product are MgO and Fe_2O_3, indicating that the magnetic product is a highly pure magnetic $MgFe_2O_4$ material. The chemical composition of the non-magnetic slag is similar to that of a cement clinker. The content of free CaO and free MgO is 0.81% and 0.68%, respectively, which improves the stability of the BOF slag and makes it applicable for use as a construction material. The synergistic oxidation process of BOF slag and copper slag achieves the goal of the comprehensive utilization of metallurgical solid waste.

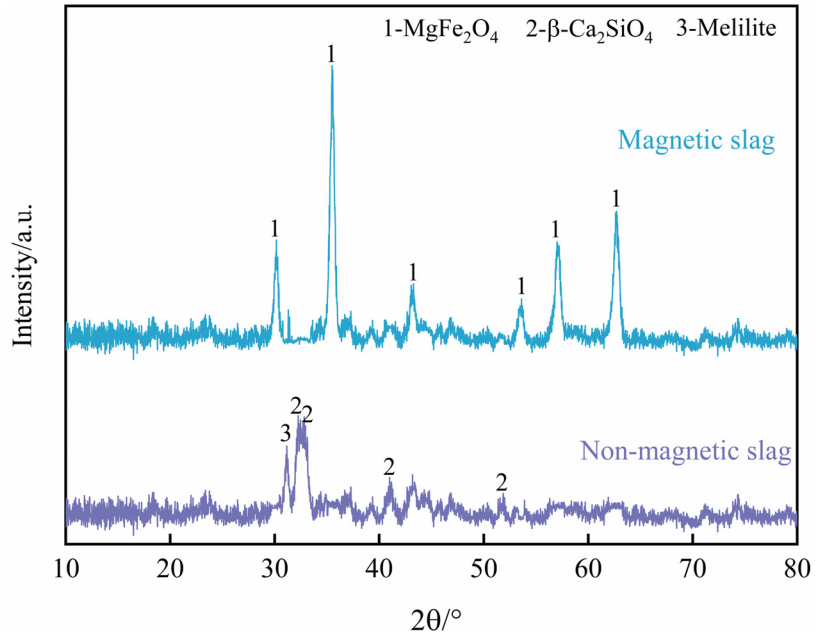


Figure 10. XRD patterns of magnetic phase and non-magnetic slag of S2 sample.

Table 4. Chemical compositions of oxidation slags (wt%).

Copper Slag Addition/Mass %	TFe	FeO	Fe_2O_3	CaO	SiO_2	MgO	Al_2O_3	MnO	P_2O_5
0	17.76	5.27	19.52	45.98	11.96	8.23	5.63	2.03	1.78
5	18.69	0.23	26.44	44.49	13.07	8.05	4.10	1.94	1.70
10	19.88	0.09	28.30	42.61	13.86	7.79	4.02	1.81	1.61
15	21.23	0.08	30.24	40.49	14.76	7.50	3.76	1.70	1.52

Table 5. Chemical composition of the product after the magnetic separation of the S2 sample (wt%).

Composition	CaO	SiO_2	MgO	FeO	Fe_2O_3	Al_2O_3	MnO	P_2O_5	f-CaO	f-MgO
Magnetic product	1.12	1.03	28.93	-	62.81	0.15	0.12	0.10	-	-
Non-magnetic slag	47.65	18.91	4.86	0.05	1.07	4.76	1.36	1.24	0.81	0.68

3. Materials and Methods

3.1. Materials

The BOF slag and copper slag used in the experiment were taken from a steelmaking company and a copper-smelting plant in China, respectively. The chemical components of the two slags are listed in Table 6. The total content in BOF slag and copper slag was 17.76% and 44.73%, respectively; this was measured by chemical titration with potassium dichromate according to the national standards of GB/T 6730.65-2009 and GB/T 6730.8-2016 [33,34]. The other components were assessed through X-ray fluorescence (XRF) analysis.

XRD analysis was used with an X-ray diffractometer (X′pert PRO, PANalytical, Netherlands) to determine the phase compositions of the BOF slag and copper slag with Cu Kα radiation (40 kV, 40 mA, wavelength 0.154 nm), and the scanned angular range varied from 10° to 80° with a scanning speed of 0.2°/s. The XRD patterns of the two slags are presented in Figure 11. The main phases of BOF slag are dicalcium silicate (Ca_2SiO_4), dicalcium ferrite ($Ca_2Fe_2O_5$), the RO phase, free lime and periclase, while copper slag consists of fayalite (Fe_2SiO_4) and magnetite (Fe_3O_4). Moreover, the content of f-CaO and f-MgO in the

BOF slag were detected by chemical extraction according to the GB/T 176-2017 national standard and the studies of Uehara et al. and Hanada et al., respectively [35–37].

Table 6. Chemical compositions of BOF slag and copper slag (wt %).

	TFe	FeO	Cu	CaO	SiO_2	MgO	Al_2O_3	MnO	P_2O_5	f-CaO	f-MgO
BOF slag	17.76	15.56	-	43.69	12.48	6.77	6.08	2.12	1.86	4.30	1.82
Copper slag	44.73	37.31	0.32	2.63	30.31	2.21	3.56	-	-	-	-

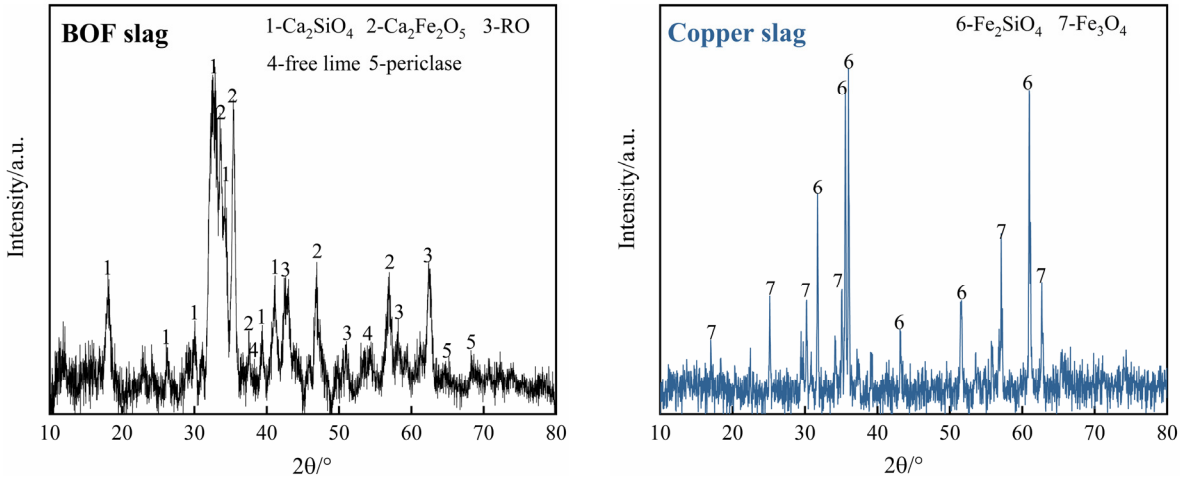


Figure 11. XRD patterns of BOF slag and copper slag.

3.2. Experimental Procedure

The oxidation experiment was carried out in a high-temperature furnace (Shanghai Jujing Precision Instrument Manufacturing Co., Ltd., Shanghai, China), as shown in Figure 12a, while Figure 12b depicts the wet magnetic separator (XCGS-50, Beijing Grand BoYu Technology Co., Ltd., Beijing, China), with a maximum magnetic flux density of 300 mT. Here, 30 g BOF slag was placed in a corundum crucible, which was placed into the constant-temperature zone of the tube furnace. The BOF slag was heated to the target temperature (1400 °C, 1450 °C and 1500 °C) to simulate the molten state of BOF slag during discharge under a high-purity argon atmosphere and held for 10 min to uniformize the slag. Then, crushed copper slag particles with granularity of less than 74 μm and oxygen gas were simultaneously injected into the molten BOF slag through the hanging corundum tube (OD 8 mm, ID 6 mm), and the flow rate of the oxygen gas was 1 L/min. The range of copper slag addition was selected as 5% to 15%. When the oxidation time (5 min, 10 min and 15 min) was reached, the crucible was taken out and cooled in air at room temperature to obtain oxidation samples. The oxidation experiment's conditions are shown in Table 7.

Next, 10 g of the oxidation slag was ground in a ball mill, and magnetic separation was carried out in a wet magnetic separator with a magnetic tube. To ensure that the particles were completely moist, the dry sample was placed in a beaker and deionized water was added. Then, we slowly poured the sample from the beaker into a magnetic separation tube filled with water, and the magnetic phase in the oxidation slag adhered to the two magnetic poles on the tube wall under the action of electromagnetism, while the non-magnetic slag was discharged outside the tube with the water flow. Following magnetic separation, the obtained materials, including the magnetic material and non-magnetic slag, were oven-dried for further examination.

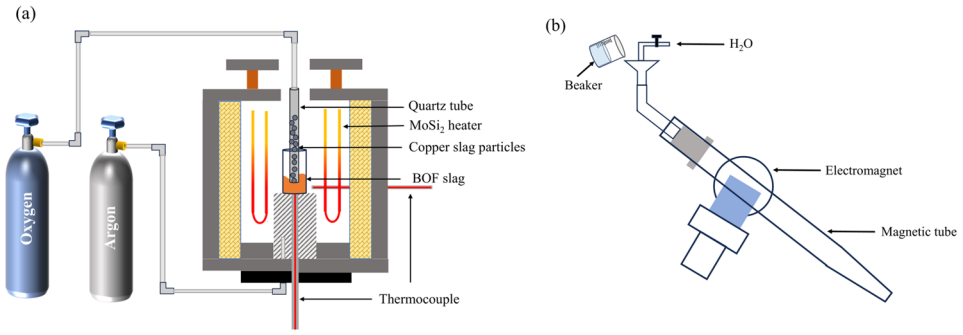


Figure 12. Schematic diagram of the experimental equipment: (**a**) high-temperature furnace; (**b**) magnetic separator.

Table 7. Oxidation experiment conditions.

Oxidation Slag Sample	Copper Slag Addition /Mass %	Oxidation Temperature/°C	Oxidation Time/min
S0	0	1450	10
S1	5	1450	10
S2	10	1450	10
S3	15	1450	10
S4	10	1400	10
S5	10	1500	10
S6	10	1450	5
S7	10	1450	15

3.3. Characterization

The synergistic oxidation process of BOF slag and copper slag converts the Fe^{2+} from the two slags to Fe^{3+}. Therefore, in order to better define the oxidation degree of Fe^{2+} in the oxidation slags, the concept of the oxidation degree is proposed in this work, as shown in Equation (5). Furthermore, the yields of magnetic $MgFe_2O_4$ following magnetic separation were determined based on Equation (6).

$$\text{Oxidation degree } (\%) = \frac{w(Fe^{2+})_m - w(Fe^{2+})_o}{w(Fe^{2+})_m} \times 100\% \quad (5)$$

$$\gamma = \frac{m_2}{m_1} \times 100\% \quad (6)$$

where $w(Fe^{2+})_m$ and $w(Fe^{2+})_o$ are the content of Fe^{2+} in the BOF slag and copper slag and the oxidation slag, respectively, %; γ is the yield of $MgFe_2O_4$, %; m_1 is the content of $MgFe_2O_4$ theoretically generated, %; and m_2 is the content of $MgFe_2O_4$ in the oxidation slag, %.

The content of TFe and Fe^{2+} in the oxidation slags was measured by chemical titration. The microstructure of the oxidation slags was characterized by scanning electron microscopy (Zeiss Ultra Plus, Germany) combined with energy-dispersive spectrometry (EDS), respectively.

4. Conclusions

The present study investigated the synergistic treatment of BOF slag and copper slag via oxidation–magnetic separation for the preparation of magnetic $MgFe_2O_4$ material and non-magnetic slag stabilization. The effects of the oxidation parameters on the phase transformation and the morphology of $MgFe_2O_4$ were also studied. The following conclusions can be drawn.

(1) The addition of copper slag can facilitate the dicalcium ferrite in BOF slag and fayalite in copper slag to release simple iron oxides of FeO and Fe_2O_3, and it promotes the formation of magnetic $MgFe_2O_4$.
(2) An increase in both the oxidation temperature and oxidation time resulted in an increase in the size of the $MgFe_2O_4$ particles, which is conducive to the separation of the magnetic $MgFe_2O_4$.
(3) The optimal oxidation conditions include 10% addition of copper slag, an oxidation temperature of 1450 °C and a 10 min oxidation time, resulting in a maximum oxidation degree of Fe^{2+} and yield of $MgFe_2O_4$ of 95.85% and 90.31%, respectively.
(4) This process results in the removal of free CaO and free MgO from the BOF slag, and the non-magnetic slag is predominantly composed of Ca_2SiO_4, which can be utilized as a construction material.

Author Contributions: Conceptualization, N.W.; methodology, N.W. and B.C.; validation, N.W. and M.C.; formal analysis, B.C.; investigation, B.C.; resources, N.W.; writing—original draft preparation, B.C.; writing—review and editing, N.W.; supervision, N.W. and M.C. All authors have read and agreed to the published version of the manuscript.

Funding: This research was funded by the National Natural Science Foundation of China, grant numbers 52274325 and 52374328.

Data Availability Statement: The data presented in this study are available on request from the corresponding author.

Conflicts of Interest: The authors declare no conflicts of interest.

References

1. He, K.; Wang, L.; Li, X. Review of the energy consumption and production structure of China's steel industry: Current situation and future development. *Metals* **2020**, *10*, 302. [CrossRef]
2. Yildirim, I.Z.; Prezzi, M. Chemical, mineralogical, and morphological properties of steel slag. *Adv. Civ. Eng.* **2011**, *2011*, 463638. [CrossRef]
3. Guo, J.; Bao, Y.; Wang, M. Steel slag in China: Treatment, recycling, and management. *Waste Manag.* **2018**, *78*, 318–330. [CrossRef] [PubMed]
4. Gao, W.; Zhou, W.; Lyu, X.; Liu, X.; Su, H.; Li, C.; Wang, H. Comprehensive utilization of steel slag: A review. *Powder Technol.* **2023**, *422*, 118449. [CrossRef]
5. Harichandan, B.; Venugopal, R. Effect of design parameters of magnetic separator on recovery of metal values from slag waste. *Int. J. Environ. Waste Manag.* **2023**, *31*, 500–513. [CrossRef]
6. Vegas, I.; Oleaga, A.; García, C.V.; Santamaria, A.; Tomas San, J.J. Assessment of steelmaking slags subjected to accelerated carbonation. *Ain Shams Eng. J.* **2024**, *15*, 102790–102804. [CrossRef]
7. Alex, T.C.; Mucsi, G.; Venugopalan, T.; Kumar, S. BOF steel slag: Critical assessment and integrated Approach for Utilization. *J. Sustain. Metall.* **2021**, *7*, 1407–1424. [CrossRef]
8. Brand, A.S.; Roesler, J.R. Steel furnace slag aggregate expansion and hardened concrete properties. *Cem. Concr. Compos.* **2015**, *60*, 1–9. [CrossRef]
9. Neto, J.B.F.; Fredericci, C.; Faria, J.O.G.; Chotoli, F.F.; Ribeiro, T.R.; Malynowskyj, A.; Silva, A.L.N.; Quarcioni, V.A.; Lotto, A.A. Modification of basic oxygen furnace slag for cement manufacturing. *J. Sustain. Metall.* **2017**, *3*, 720–728. [CrossRef]
10. Naakase, K.; Matsui, A.; Nakai, Y.; Kikuchi, N.; Kishimoto, Y.; Tetsuyama, I. Development of Iron Recovery Technique from Steelmaking Slag by Reduction at High Temperature. *ISIJ Int.* **2023**, *63*, 429–435. [CrossRef]
11. Harada, T.; Hirata, H.; Arai, T.; Toh, T.; Yamada, T. Development of the Molten Slag Reduction Process-1 Characteristics of Closed Type DC arc Furnace for Molten Slag Reduction. *ISIJ Int.* **2018**, *58*, 1934–1942. [CrossRef]
12. Guo, H.; Yin, S.; Yu, Q.; Yang, X.; Huang, H.; Yang, Y.; Gao, F. Iron recovery and active residue production from basic oxygen furnace (BOF) slag for supplementary cementitious materials. *Resour. Conserv. Recycl.* **2018**, *129*, 209–218. [CrossRef]
13. Hao, S.; Luo, G.; Wang, L.; An, S.; Chai, Y.; Song, W. Preparation of cementing material and recovery of iron resources using converter slag. *Process. Saf. Environ. Prot.* **2024**, *190*, 73–84. [CrossRef]
14. Dai, W.; Li, Y.; Cang, D.; Liu, Z.; Fan, Y. BOF Slag Glass-ceramics Prepared in Different Atmospheres from Parents Glasses with Various Reduction Degree. *ISIJ Int.* **2014**, *54*, 2672–2677. [CrossRef]

15. Lan, M.; He, Z.; Hu, X. Optimization of Iron Recovery from BOF Slag by Oxidation and Magnetic Separation. *Metals* **2022**, *12*, 742. [CrossRef]
16. Xue, P.; He, D.; Xu, A.; Gu, Z.; Yang, Q.; Engström, F.; Björkman, B. Modification of industrial BOF slag: Formation of $MgFe_2O_4$ and recycling of iron. *J. Alloys Compd.* **2017**, *712*, 640–648. [CrossRef]
17. He, Z.; Hu, X.; Chou, K.-C. Oxidative modification of industrial basic oxygen furnace slag for recover iron-containing phase: Study on phase transformation and mineral structure evolution. *Process. Saf. Environ.* **2023**, *171*, 167–175. [CrossRef]
18. Li, Y.; Dai, W. Modifying hot slag and converting it into value-added materials: A review. *J. Clean. Prod.* **2018**, *175*, 176–189. [CrossRef]
19. Tian, H.; Guo, Z.; Pan, J.; Zhu, D.; Yang, C.; Xue, Y.; Li, S.; Wang, D. Comprehensive review on metallurgical recycling and cleaning of copper slag. *Resour. Conserv. Recycl.* **2021**, *168*, 105366. [CrossRef]
20. Cao, B.; Wang, N.; Zhang, C.; Chen, M. Co-modification of BOF slag and copper slag to recover valuable metals by carbothermal reduction. *JOM* **2023**, *75*, 3568–3576. [CrossRef]
21. Jamal Uddin, M.; Jeong, Y.K. Application of magnesium ferrite nanomaterials for adsorptive removal of arsenic from water: Effects of Mg and Fe ratio. *Chemosphere* **2022**, *307*, 135817. [CrossRef] [PubMed]
22. Kaur, N.; Kaur, M.; Singh, D. Fabrication of mesoporous nanocomposite of graphene oxide with magnesium ferrite for efficient sequestration of Ni (II) and Pb (II) ions: Adsorption, thermodynamic and kinetic studies. *Environ. Pollut.* **2019**, *253*, 111–119. [CrossRef] [PubMed]
23. Shu, R.; Zhao, Z.; Yang, X. Fabrication of nitrogen-doped reduced graphene oxide/porous magnesium ferrite@silica dioxide composite with excellent dual-band electromagnetic absorption performance. *Chem. Eng. J.* **2023**, *473*, 145224. [CrossRef]
24. Liu, C.; Huang, S.; Blanpain, B.; Guo, M. Optimization of mineralogy and microstructure of solidified basic oxygen furnace slag through SiO_2 addition or atmosphere control during hot-stage slag treatment. *Metall. Mater. Trans. B* **2018**, *50*, 210–218. [CrossRef]
25. Tian, T.; Li, G.; Li, Y.; Li, T.; Yuan, C.; Liu, Y. Thermodynamics and kinetics on hot state modification of BOF slag by adding SiO_2. *Metall. Mater. Trans. B* **2023**, *54*, 1131–1143. [CrossRef]
26. Talero, R.; Trusilewicz, L.; Delgado, A.; Pedrajas, C.; Lannegrand, R.; Rahhal, V.; Mejía, R.; Delvasto, S.; Ramírez, F.A. Comparative and semi-quantitative XRD analysis of Friedel's salt originating from pozzolan and Portland cement. *Constr. Build. Mater.* **2011**, *25*, 2370–2380. [CrossRef]
27. Cuevas, J.; Cabrera, M.Á.; Fernández, C.; Mota-Heredia, C.; Fernández, R.; Torres, E.; Turrero, M.J.; Ruiz, A.I. Bentonite Powder XRD Quantitative Analysis Using Rietveld Refinement: Revisiting and Updating Bulk Semiquantitative Mineralogical Compositions. *Minerals* **2022**, *12*, 772. [CrossRef]
28. Lin, Y.; Liu, Y.; Chou, K.; Shu, Q. Effects of oxygen atmosphere, FeOx and basicity on mineralogical phases of $CaO–SiO_2–MgO–Al_2O_3–Fe_tO–P_2O_5$ steelmaking slag. *Ironmak. Steelmak.* **2018**, *46*, 1470362. [CrossRef]
29. Ma, Y.; Du, X. Influence of CaO addition, FeO/SiO_2, and MgO/SiO2 on the melting characteristic temperatures of FeO-SiO_2-MgO-CaO System. *Mater. Res.* **2019**, *22*, e20180645. [CrossRef]
30. Duée, C.; Bourgel, C.; Véron, E.; Allix, M.; Fayon, F.; Bodénan, F.; Poirier, J. Phosphorus speciation in dicalcium silicate phases: Application to the basic oxygen furnace (BOF) slag. Cem. *Concr. Res.* **2015**, *73*, 207–214. [CrossRef]
31. Gautier, M.; Poirier, J.; Bodénan, F.; Franceschini, G.; Véron, E. Basic oxygen furnace (BOF) slag cooling: Laboratory characteristics and prediction calculations. *Int. J. Miner. Process.* **2013**, *123*, 94–101. [CrossRef]
32. Andreozzi, G.B.; Lucchesi, S. Intersite distribution of Fe^{2+} and Mg in the spinel (sensu stricto)–hercynite series by single-crystal X-ray diffraction. *Am. Miner.* **2002**, *87*, 1113–1120. [CrossRef]
33. *GB/T 6730.65-2009*; Iron Ores—Determination of Total Iron Content-Titanium (III) Chloride Reduction Potassium Dichromate Titration Methods (Routine Methods). Standards Press of China: Beijing, China, 2009.
34. *GB/T 6730.8-2016*; Iron Ores—Determination of Iron (II) Content—Potassium Dichromate Titrimetric Method. Standards Press of China: Beijing, China, 2016.
35. *GB/T 176-2017*; Methods for Chemical Analysis of Cement. Standards Press of China: Beijing, China, 2017.
36. Uehara, N.; Takita, M. Extraction of free magnesia from steelmaking slags using Iodine–Ethanol solutions. *ISIJ Int.* **2018**, *58*, 1474–1479. [CrossRef]
37. Hanada, K.; Inose, M.; Sato, S.; Watanabe, K.; Fujimoto, K. Development of analytical methods for free-MgO in steelmaking slag. *Tetsu Hagane-J. Iron Steel Inst. Jpn.* **2016**, *102*, 24–28. [CrossRef]

Disclaimer/Publisher's Note: The statements, opinions and data contained in all publications are solely those of the individual author(s) and contributor(s) and not of MDPI and/or the editor(s). MDPI and/or the editor(s) disclaim responsibility for any injury to people or property resulting from any ideas, methods, instructions or products referred to in the content.